Journal of Power Sources 207 (2012) 10–18

Contents lists available at SciVerse ScienceDirect

Journal of Power Sources

journal homepage: www.elsevier.com/locate/jpowsour

Interpretation of processes at positive and negative electrode by measurement and simulation of impedance spectra. Part I: Inductive semicircles☆

Julia Kowal*, Heide Budde-Meiwes, Dirk Uwe Sauer

Electrochemical Energy Conversion and Storage Systems, Institute for Power Electronics and Electrical Drives (ISEA), RWTH Aachen University, Germany

ARTICLE INFO

Article history:
Received 22 September 2011
Accepted 8 December 2011
Available online 17 December 2011

Keywords:
Lead-acid battery
Impedance spectroscopy
Inductive semicircle
Modelling

ABSTRACT

Impedance measurements of both electrodes of a flooded OEM SLI battery at various SOC and with various direct currents have been measured. For each part of the impedance spectra, an electrochemical process is proposed and implemented in a simulation model. By simulation of impedance spectroscopy, spectra of the model are obtained and compared with the measurement. In this first part, the focus is put on inductive semicircles in impedance spectra.

1. Introduction

Measured impedance spectra of electrodes of lead-acid batteries (Fig. 1) reveal that both electrodes are capacitive (negative imaginary part) in a wide frequency range, as expected, but also inductive (positive imaginary part) in certain frequency ranges. The so-called inductive branch at high frequencies can be explained from geometry effects. Besides this inductive branch, the negative electrode shows a so-called inductive semicircle at low frequencies (about 10 mHz and below) and the positive electrode sometimes shows an inductive semicircle at frequencies higher than the intersection point with the real axis (between 10 Hz and some 100 Hz). A semicircle is called inductive if it has positive imaginary values. Using lumped elements, such a semicircle can be modelled with a positive inductance or a negative capacitance. At the negative electrode, the inductive semicircle occurs at low frequencies, which is a reason against inductance because inductances are typically important at high frequencies. On the other hand, a negative capacitance is rather hard to imagine for a physical or chemical process, so both cases seem to be unlikely. Additionally, the resistance in parallel to a negative capacitance needs to be negative as well, which is also hard to explain. The aim of this work has therefore been to identify and to model physical or chemical processes causing such inductive semicircles.

2. Impedance spectra of lead-acid battery electrodes

The impedance of complete lead-acid batteries, positive and negative electrodes as well as of lead and lead dioxide has been studied under various conditions. An extensive literature survey until 2001 can be found in the dissertation of Karden [1].

2.1. Negative electrode

Typical impedance spectra of the negative electrode are shown in Fig. 2. At high frequencies, the spectrum consists of an inductive branch, which is slightly bent. Between 200 and 800 Hz, the spectrum intersects with the real axis and continues with two capacitive semicircles, the high-frequency semicircle in the 10 Hz range and the low-frequency semicircle in the 0.1 Hz range. In the 10 mHz range, the spectrum often becomes inductive again with an inductive semicircle. At even lower frequencies, the spectrum can exhibit a straight line, but Kramers–Kronig check[1] reveals that this is caused by instationary behaviour and should not be interpreted. At 90% SOC, the impedance rises with a 45° angle after the first capacitive semicircle, which indicates a diffusion limitation. This inclination can either be the beginning of a second capacitive semicircle (diffusion in pores) or a continuous straight line (bulk diffusion).

☆ This paper was presented at 8th International LABAT Conference 2011 in Albena, Bulgaria.

* Corresponding author. Tel.: +49 241 8096935; fax: +49 241 8092203.
E-mail addresses: batteries@isea.rwth-aachen.de, sf@isea.rwth-aachen.de (J. Kowal).

[1] Impedance spectroscopy does only give reasonable results if three conditions are fulfilled: linearity, time invariance and causality. Minor violations of linearity and time invariance are tolerable, which is then called quasi-linear or quasi-stationary. If the violations are within tolerable limits can be tested with the Hilbert or Kramers–Kronig transform [67–69].

0378-7753/$ – see front matter © 2011 Elsevier B.V. All rights reserved.
doi:10.1016/j.jpowsour.2011.12.015

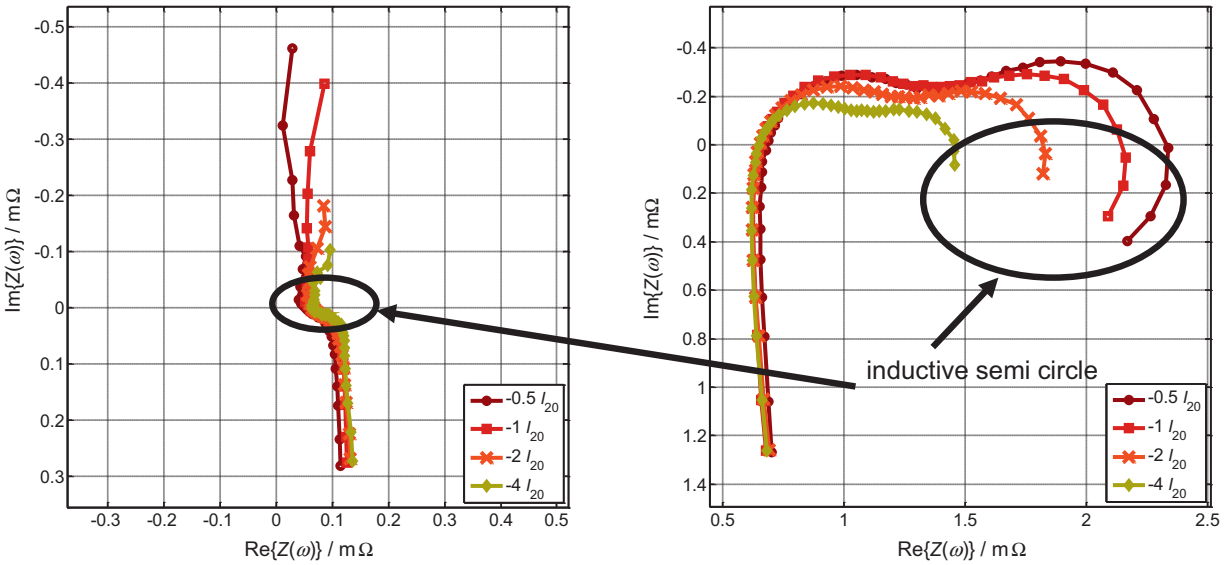

Fig. 1. Impedance spectra of positive (left) and negative electrode (right) of a 60 Ah flooded lead-acid battery at 40% SOC at 25 °C with different superposed direct currents. The SOC was adjusted by discharging. Inductive semicircles are indicated.

It is generally agreed that the origin of the inductive branch is the geometry of the cell, see e.g. [1–6]. The inclination of the inductive branch can be attributed to the skin effect or current displacement [7]. It can be seen that the series resistance, which can be read approximately from the intersection with the real axis, increases with depth of discharge. It is caused by the limited conductivity of all components of the battery. The dependence on state of charge originates from the acid-density dependence of the electrolyte resistance and the decreasing cross-section for the electrochemical reaction due to the coverage by lead sulphate [2,3,8,9].

All semicircles must be connected with the processes connected to the electrode reactions. Charge-transfer processes together with the double-layer capacitance result in capacitive semicircles [10]. Hence, one of the capacitive semicircles probably represents the charge-transfer process. A 45° slope at the beginning of the high-frequency semicircle indicates diffusion in pores. Fig. 3 shows the current dependency of the semicircles at 70% SOC. It can be seen that the low-frequency capacitive semicircle and the inductive semicircle are much more current dependent and change with the same factor, while the high-frequency semicircle does not change much with current. All three semicircles depend on SOC (Fig. 2). The current dependency of the low-frequency semicircles suggests their connection to charge transfer.

In literature, various interpretations of the two capacitive and one inductive semicircle are given. Only few researchers measured the inductive semicircle [1,4,5,11], but most of them do not comment on them. Others only measured down to frequencies in the Hz range, so they could not observe this semicircle. Yahchouchi [6] attributed the high-frequency capacitive semicircle to the porous surface and surface coverage by lead sulphate and the low-frequency capacitive semicircle to the charge-transfer reaction, while the interpretation of Mauracher and Karden [12] was vice versa. According to Huet [2], the high-frequency capacitive semicircle of a cell spectrum is related to the porous structure of both electrodes and the low-frequency capacitive semicircle is caused by the sulphation reaction limited by Pb^{2+} ions. Stoynov et al. [5] attributed the capacitive semicircles to nucleation and the inductive semicircle to propagation. Lindbergh [13] related the increasing semicircle of a porous lead electrode with depth of discharge to the decreasing active surface. He used the

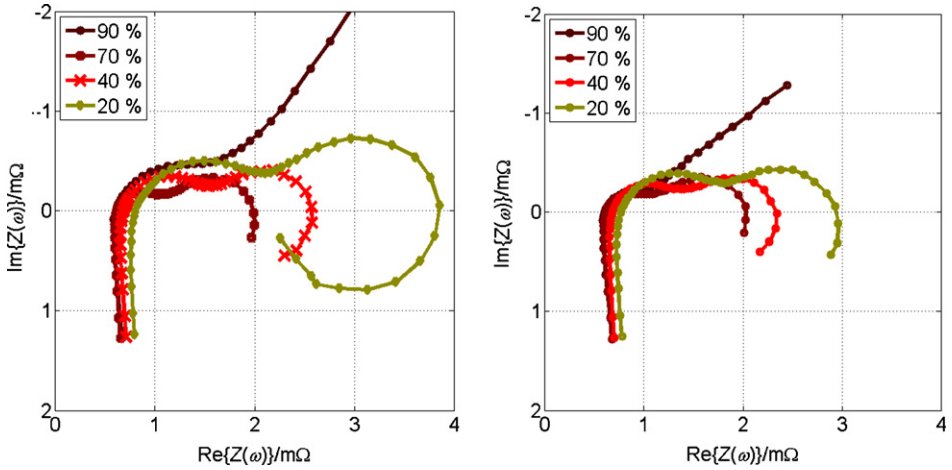

Fig. 2. Impedance spectra during charging (left) and discharging (right) of the negative electrode of a 60 Ah flooded lead-acid battery at different SOC at 25 °C, superposed direct current is ±0.5 I_{20} and the SOC was adjusted by discharging. Measured frequencies are between 6 kHz and 3 mHz with eight frequencies per decade. Points that do not pass Kramers–Kronig consistency check are not shown; the complete spectra are depicted in Part II of this paper.

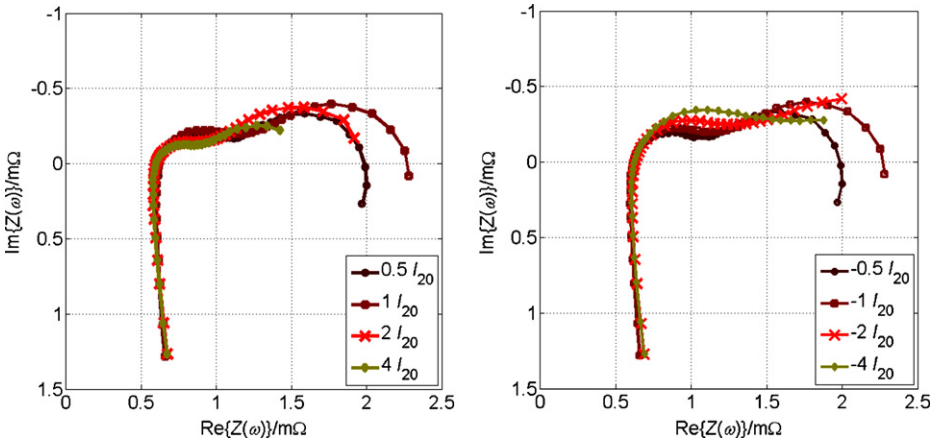

Fig. 3. Impedance spectra during charging (left) and discharging (right) of the negative electrode of a 60 Ah flooded lead-acid battery at 70% SOC at 25 °C with different superposed direct currents. The SOC was adjusted by discharging. Measured frequencies are between 6 kHz and 3 mHz ($\pm 0.5 I_{20}$), 5 mHz ($\pm I_{20}$), 11 mHz ($\pm 2 I_{20}$) or 19 mHz ($\pm 4 I_{20}$) with eight frequencies per decade. Points that do not pass Kramers–Kronig consistency check are not shown.

pore-impedance formulation by de Levie [14–17] together with charge-transfer impedance as interface impedance, which fits the experimental data quite well. Beketaeva and Rybalka [18] measured the impedance and porosity of the negative active mass in different depths of discharge and could relate the pore volume with the real part of the impedance (first semicircle). Kirchev et al. [4] interpreted the high-frequency semicircle as the parallel connection of charge-transfer resistance and double-layer capacitance and the low-frequency semicircle as the adsorption impedance, another RC parallel connection, representing the transport of Pb^{2+} ions from the pore to the adsorption layer in the outer Helmholtz layer. They also observed an inductive semicircle, but no interpretation is given. D'Alkaine et al. [19] attributed the high-frequency semicircle to reactions in the pores and the low-frequency semicircle to inhomogeneous current distribution. Niya et al. [20] found no inductive semicircle, but attributed the two capacitive semicircles to charge transfer combined with sulphate layer formation including adsorption and mass transfer.

2.2. Positive electrode

Fig. 4 shows typical impedance spectra of a positive electrode. The beginning of a large semicircle is observable at frequencies below 10 Hz. Often the real part becomes negative. Such behaviour could be interpreted as indication of depletion (see Part II of this paper). The interpretation of the series resistance at the intersection of the real axis is similar to that of the negative electrode. Also similar to the negative electrode, the high-frequency behaviour shows an inductive line, which can be inclined towards increasing real part instead of being completely vertical.

Sometimes a small inductive semi circle is observable in the range from 10 Hz to 300 Hz (Fig. 5), which does not fit to the skin effect or current displacement theory that would only explain the inclination. Such an inductive semi circle has also been measured, but not commented, by Yahchouchi [6]. In a series of papers, Hampson and co-workers from the Loughborough University of Technology, England, presented impedance measurements of solid and porous lead dioxide on different alloys [21–26]. In their measurements, such an inductive semicircle occurred on porous lead dioxide and if grid alloys with antimony content are used, but only at high potentials equivalent to a fully charged electrode. So they concluded that antimony makes the surface more porous. Porosity as the origin for inductive behaviour was later disproved by Keddam et al. [27]. Kirchev et al. [28] measured the impedance of positive electrodes during charge/discharge cycles in electrolyte with 1.24 g cm^{-3} and 1.28 g cm^{-3} at various SOC. In some spectra, they also found an inductive high-frequency semicircle, which they attributed to slowed-down chemical reactions inside the pores. This semicircle occurs both after charging and discharging in 1.28 g cm^{-3}, but only after charging in 1.24 g cm^{-3}. Several authors [29–32] have shown that such a high-frequency inductive semicircle can be caused by the reference electrode (see Section 3.2). The effect can be shifted to higher frequencies by changing the electrolyte concentration or the measurement setup. Fig. 5 shows that the size of the semicircle depends on SOC and is more or less independent from current. Acid concentration changes with SOC, so this is the most probable explanation for this semicircle. Further measurements with different reference electrodes and different setups are planned to investigate this in future.

3. Origin of inductive semicircles

An inductive semicircle (see Fig. 1) can either be caused by a positive resistance and inductance or a negative resistance and capacitance. Although it seems impossible to have a negative resistance, it must be kept in mind that the measured (small signal) impedance is only a derivative of the actual (large signal) resistance characteristic, which means that a measured negative real part of impedance only indicates a negative slope.

In literature, possible origins of inductive semicircles are electrochemical processes such as adsorption or desorption of reactants or blocking particles, passivation layer, slow charge relaxation in two-phase materials or slow nucleation. Besides that, if reference electrodes are used, high-frequency inductive semicircles can be caused by the geometry of the reference electrode or the measurement setup.

3.1. Adsorption

Many authors have ascribed pseudoinductive behaviour in electrochemical processes to adsorption: Gutmann [33] found that it can be caused by negative $d\theta/d\eta$ due to adsorption, where θ is the coverage with adsorbed particles and η is the overpotential. de Levie and Husovsky [34] ascribed their findings to charge-transfer reactions with adsorbed ligands instead of ions. In a mathematical analysis, Sadkowski [35] found that negative capacitances could arise if strong adsorption is involved. He further investigated theoretically mathematical criteria for stability and the distinction

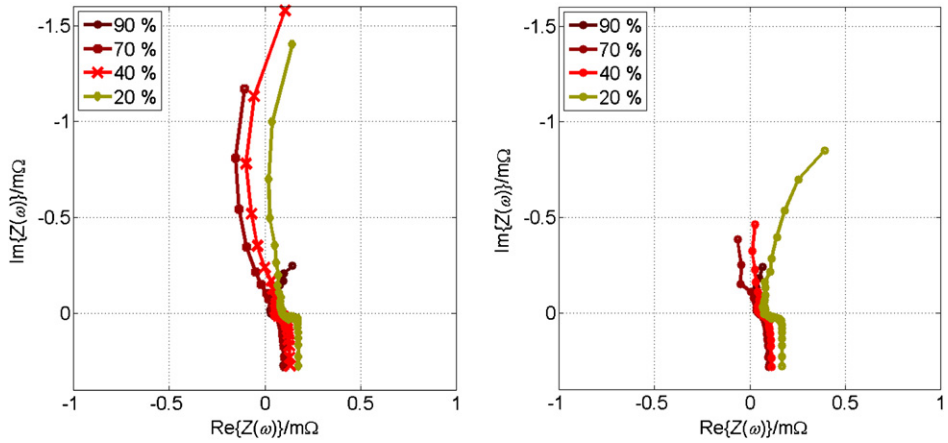

Fig. 4. Impedance spectra during charging (left) and discharging (right) of the positive electrode of a 60 Ah flooded lead-acid battery at different SOC at 25 °C, superposed direct current is $\pm 0.5\ I_{20}$. The SOC was adjusted by discharging. Measured frequencies are between 6 kHz and 3 mHz with eight frequencies per decade. Points that do not pass Kramers–Kronig consistency check are not shown; the complete spectra are depicted in Part II of this paper.

between capacitive and inductive behaviour [36–38] and attributed the inductive behaviour to the autocatalytic mechanisms of adsorption, which means that an increase in surface coverage stimulates further increase. Bai and Conway [39,40] theoretically analysed the case of pseudoinductive behaviour caused by passivation with negative $d\theta/d\eta$ for one and two adsorbed intermediates. In the case of two adsorbed intermediates, two pseudoinductive semicircles occur if the slope $d\theta/d\eta$ of both species is negative. Koper [41] derived mathematically three possibilities for negative resistances from the Butler–Volmer equation (see Eq. (1), surface area A, coverage θ, reaction rate k and concentration c are included in i_0):

- $dA/d\eta < 0$ or $d\theta/d\eta < 0$, which means that the surface area A decreases with increasing potential, such as increased surface coverage by a passivating layer with increasing potential.
- $dk/d\eta < 0$, caused e.g. by adsorption of an inhibitor that either blocks the surface (case 1) or increases the free enthalpy ΔG
- $dc/d\eta < 0$, which is possible for a low concentration electrolyte.

Bisquert et al. [42] gave an overview of the origin of inductive behaviour in different kinds of systems. In electrochemical reactions, inductive behaviour occurs if the concentration of adsorbed species rises at falling potential and at high charge-transfer current.

3.2. Reference electrode

A high-frequency (>100 Hz) inductive semicircle can also be caused by the reference electrode in a setup with two working electrodes and a reference electrode. Göhr et al. [30] and Chechirlian et al. [29] measured the influence of the reference electrode on impedance spectra for different reference electrodes and derived a theoretical model. Stray capacitances and inductances between the three electrodes as well as finite electrolyte conductivity and reference electrode resistance are the cause for the distortion. Type and geometry of the reference electrode and its distance to the measured electrode have a large influence on the shape of the impedance diagram as well as electrolyte concentration because it changes electrolyte conductivity [29]. Increasing electrolyte conductivity, increasing distance between working and reference electrode or shielding of the reference electrode shifts the artefacts to higher frequencies [30]. Reference electrode designs with reduced influence were proposed by Göhr et al. [30] and Schiller and Strunz [32].

As already mentioned in Section 2.2, this is the most probable origin of the inductive semicircle at the positive electrode.

4. Simulation

In this section, the different parts of the impedance spectrum of the negative electrode of lead-acid batteries are discussed.

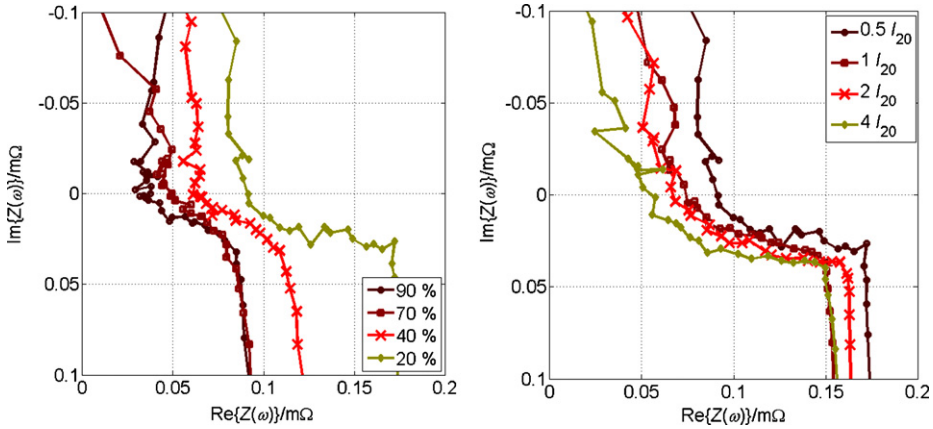

Fig. 5. High-frequency inductive semicircle of positive electrode; left: different SOC during charging with $0.5 I_{20}$ (zoom of Fig. 4 left); right: different charging currents at 20% SOC; SOC was adjusted by discharging.

First of all, the impedance of a simple charge transfer reaction is derived, which is then extended with adsorption and desorption. Afterwards, an interpretation of the high-frequency capacitive semicircle is given. Simulated impedance spectra with the derived equations are compared with the measured spectra. All derivations of equations and the method how to determine the impedance formulations can be found in [43].

Throughout this section, impedance parameters are chosen to generate impedance spectra corresponding to the electrodes of a 60 Ah flooded SLI battery. The currents that are used for simulation are given in multiples of $I_{20} = 3$ A.

4.1. Charge transfer

The simplest electrode process is charge transfer without concentration limitation or other coupled processes and is described with the basic Butler–Volmer equation[2]:

$$i_{ct} = -i_0 \cdot \left(\exp\left(\frac{\alpha \cdot n \cdot F}{R \cdot T} \cdot \eta\right) - \exp\left(-\frac{(1-\alpha) \cdot n \cdot F}{R \cdot T} \cdot \eta\right)\right) \quad (1)$$

i_0 is the exchange current, α is the symmetry coefficient, n is the number of exchanged electrodes, $F = 96{,}485$ As mol^{-1} is the Faraday constant, $R = 8.314$ J mol^{-1} K^{-1} is the gas constant and T is the temperature in K. Charge transfer occurs in parallel to the double-layer capacitance C_{DL}, thus the total current is the sum of Eq. (1) and the current through the double-layer capacitance:

$$i = i_{ct} + i_{DL} = -i_0 \cdot \left(\exp\left(\frac{\alpha \cdot n \cdot F}{R \cdot T} \cdot \eta\right) - \exp\left(-\frac{(1-\alpha) \cdot n \cdot F}{R \cdot T} \cdot \eta\right)\right) + C_{DL} \cdot \frac{d\eta}{dt} \quad (2)$$

The resulting small-signal impedance $\underline{Z}_{ssi}(\omega, \eta_{DC})$ is:

$$\underline{Z}_{ssi}(\omega, \eta_{DC}) = \frac{1}{i_0 \cdot ((\alpha nF/RT) \cdot \exp((\alpha nF/RT)\eta_{DC}) + ((1-\alpha)nF)/RT \cdot \exp(-((1-\alpha)nF/RT)\eta_{DC})) + j\omega C_{DL,lsi}(\eta_{DC})} \quad (3)$$

4.2. Charge transfer in combination with adsorption/desorption

It is assumed that the product of the charge-transfer reaction during discharge does not directly dissolve in the electrolyte, but first stays in an adsorption site and is then desorbed and dissolved. During charging, the ions first have to be adsorbed to the electrode before they can take part in the charge-transfer reaction. Such a two-step mechanism could take place at the negative electrode of the lead-acid battery [20]. Several authors have mentioned that adsorption of different ions takes place at the negative electrode [44–53]. Vanmaekelbergh and Erné [54] derived a model for metal dissolution that consists of those two steps with similar results as those presented in the following.

The assumed course of reaction is illustrated in Fig. 6. After charge transfer (step 1), the resulting lead ion is not directly dissolved from the lattice to the electrolyte, but first moved to a surface lattice (adsorption) site to be desorbed in step 2. Step 3 is the (chemical) sulphation reaction, which is not directly visible in the impedance spectra, only if concentration limitation becomes significant.

If it is further assumed that charge transfer in charge direction can only take place at the surface covered with adsorbed ions and in discharge direction at the uncovered surface, surface coverage influences the charge-transfer reaction and also the impedance. The corresponding Butler–Volmer equation is given as:

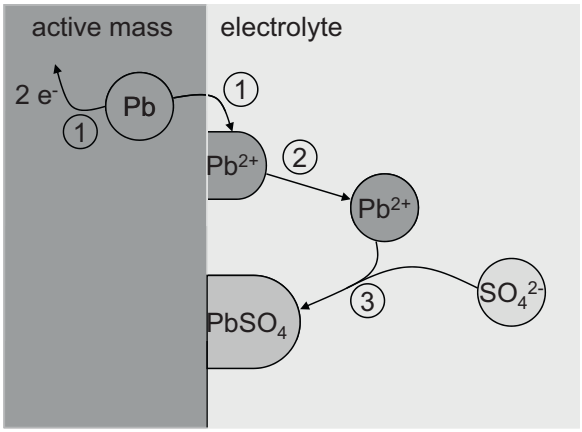

Fig. 6. Illustration of discharge processes at the negative electrode of a lead-acid battery. 1: charge transfer; 2: desorption; and 3: chemical reaction (not directly visible in a Nyquist plot). During charging, the reverse processes take place.

$$i(t) = -i_0 \cdot \left((1-\theta(t)) \cdot \exp\left(\frac{\alpha nF}{RT}\eta(t)\right) - \theta(t) \cdot \exp\left(-\frac{(1-\alpha)nF}{RT}\eta(t)\right)\right) \quad (4)$$

The surface coverage $\theta(t) = \Gamma(t)/\Gamma_{max}$ is defined as the current surface ion concentration $\Gamma(t)$ divided by the maximum surface concentration Γ_{max}. This assumes as simplification that the surface is completely covered if $\Gamma(t) = \Gamma_{max}$. θ and $1-\theta$ are illustrated in Fig. 7.

Surface coverage changes both with the charge transfer and the adsorption/desorption process[3]:

$$\frac{d\theta(t)}{dt} = k_{ct} \cdot \left((1-\theta(t)) \cdot \exp\left(\frac{\alpha nF}{RT}\eta(t)\right) - \theta(t) \cdot \exp\left(-\frac{(1-\alpha)nF}{RT}\eta(t)\right)\right) - k_{desad} \cdot \left(\theta(t) \cdot \exp\left(\frac{\beta nF}{RT}\eta(t)\right) - (1-\theta(t)) \cdot \exp\left(-\frac{(1-\beta)nF}{RT}\eta(t)\right)\right) \quad (5)$$

k_{ct} and k_{desad} are the rate constant of the charge transfer and the adsorption/desorption process, respectively, and α and β the corresponding symmetry coefficients.

The small signal impedance (ssi) of such a process is of the form[4]

$$\underline{Z}_{ssi}(\omega, \eta_{DC}) = \frac{1}{(-A(\eta_{DC}))/(j\omega + B(\eta_{DC})) + D(\eta_{DC}) + j\omega C_{DL}} \quad (6)$$

The abbreviations $A(\eta_{DC})$, $B(\eta_{DC})$ and $D(\eta_{DC})$ are given in Appendix A. C_{DL} is the double layer capacitance. Eq. (6) corresponds to the electrode impedance depicted in Fig. 8 with

$$R_{ct,ssi}(\eta_{DC}) = \frac{1}{D(\eta_{DC})} \quad (7)$$

[2] In lead-acid batteries the positive electrode has a positive equilibrium potential against reference and the negative electrode has a negative equilibrium potential against reference. The negative sign here is needed for the negative electrode; for a positive electrode, the sign is inverted.

[3] It is assumed here that the potential of zero charge ϕ_{pzc} is zero. Strictly speaking, in the second term of Eq. (5), $\eta(t)$ should be replaced by $\eta(t) - \phi_{pzc}$. However, ϕ_{pzc} does not depend on η or θ, so this change would only add a constant factor to both exponential terms and would not change the general characteristics of the following equations.

[4] The method how to determine the small signal impedance is described in [70,43].

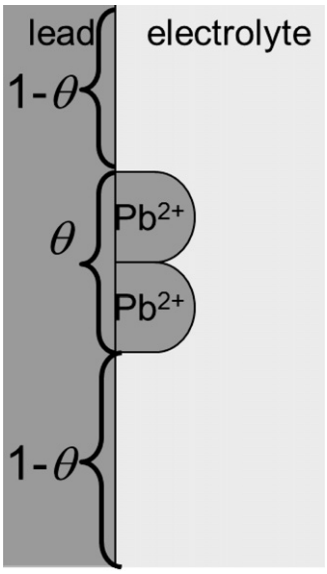

Fig. 7. Illustration of surface coverage θ, which is the covered surface fraction, and $1-\theta$, which is the uncovered surface fraction.

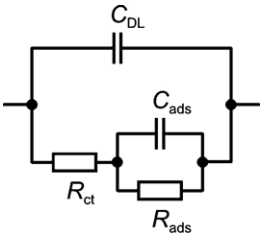

Fig. 8. Equivalent circuit describing charge transfer with coupled adsorption.

$$R_{\mathrm{ads,ssi}}(\eta_{\mathrm{DC}}) = \frac{A(\eta_{\mathrm{DC}})}{D(\eta_{\mathrm{DC}}) \cdot (D(\eta_{\mathrm{DC}}) \cdot B(\eta_{\mathrm{DC}}) - A(\eta_{\mathrm{DC}}))} \tag{8}$$

$$C_{\mathrm{ads,ssi}}(\eta_{\mathrm{DC}}) = \frac{D^2(\eta_{\mathrm{DC}})}{A(\eta_{\mathrm{DC}})} \tag{9}$$

The resulting impedance spectrum consists of two semicircles, where the one at lower frequencies can be capacitive or inductive depending on the parameters. $B(\eta_{\mathrm{DC}})$, $D(\eta_{\mathrm{DC}})$ and consequently also $R_{\mathrm{ct,ssi}}(\eta_{\mathrm{DC}})$ are always larger than zero. As they determine the semicircle at higher frequencies, it is always capacitive. $A(\eta_{\mathrm{DC}})$ can both be negative and positive. The sign of $A(\eta_{\mathrm{DC}})$ also determines the sign of $R_{\mathrm{ads,ssi}}(\eta_{\mathrm{DC}})$ and $C_{\mathrm{ads,ssi}}(\eta_{\mathrm{DC}})$. Hence, if $A(\eta_{\mathrm{DC}})$ is negative, the lower-frequency semicircle is inductive and if it is positive, the semicircle is capacitive.

This is illustrated in the following with two exemplary sets of parameters. All parameters are the same in both sets besides k_{ct} and k_{desad}, which determine the surface coverage with lead ions (Eq. (5)). Fig. 9 shows the resulting spectra. With this set of parameters, one capacitive and one inductive semicircle are observable if $k_{\mathrm{desad}} > k_{\mathrm{ct}}$ (Fig. 9 left). The corresponding spectra with $k_{\mathrm{ct}} > k_{\mathrm{desad}}$ leading to two capacitive semicircles are shown in the right-hand picture of Fig. 9. However, because of the complicated structure of $A(\eta_{\mathrm{DC}})$ and its dependence on α, β, k_{ct}, k_{desad} and η_{DC}, $A(\eta_{\mathrm{DC}})$ is not generally negative if $k_{\mathrm{desad}} > k_{\mathrm{ct}}$, but all five parameters have to be taken into account.

$k_{\mathrm{desad}} > k_{\mathrm{ct}}$ means that adsorption and desorption are faster than charge transfer, implicating that it takes a longer time to integrate or remove ions into or from the lattice than to attach to or dissolve ions to or from an adsorption site. In other words, the surface coverage θ increases faster during charging and slower during discharging. During charging, the overvoltage η is smaller than zero and larger than zero during discharging. This means that $\mathrm{d}\theta/\mathrm{d}\eta < 0$, which is the most frequently stated criterion for inductive semicircles in literature, e.g. [39–41]. $K_{\mathrm{ct}} > k_{\mathrm{desad}}$ results in $\mathrm{d}\theta/\mathrm{d}\eta > 0$, which causes capacitive semicircles.

4.3. Negative electrode

As described in Section 2.1, the impedance spectrum of the negative electrode consists of an inductive branch at high frequencies, two capacitve semi circles at intermediate frequencies and an inductive semi circle at low frequencies. For the capacitive semicircles, several possible explanations can be found in literature. Electrode processes resulting in capacitive semicircles are charge transfer, chemical reactions and adsorption (see chapter 3). Most probably, charge transfer as well as adsorption occurs in only one rate-limiting step each,[5] so those processes can be described by the two other semicircles as described in Section 4.2. The remaining process depicted in Fig. 6 is the (chemical) sulphation reaction in combination with crystallisation and corresponding coverage of the active surface, which could be a possible explanation for the second capacitive semi circle. However, simulations have shown that this possibility is quite unlikely. As the sulphationreaction does not depend on potential, it is hardly visible in the impedance spectrum, only as concentration limitation (see Part II of this paper).

Another cause for a capacitive semicircle is a coating on the electrode surface, which can be modelled by an RC parallel connection in series to the remaining impedance or in a nested circuit. Several authors [55–61] have mentioned that at the very beginning of the discharge a thin lead-sulphate film penetrable for Pb^{2+} ions forms on the electrode surface. The surface is completely covered within seconds. This is depicted in Fig. 10, which is Fig. 6 with an additional lead-sulphate film between lead (active mass) and sulphuric acid (electrolyte).

This adds a resistance and capacitance to the reaction path and could be the origin of the high-frequency semicircle. In literature, two kinds of coatings are distinguished: continuous or defect-less coating and discontinuous coating or coating with defects. The first kind is typically modelled with an RC parallel connection in series (Fig. 11 left) and the second kind with the nested circuit (Fig. 11, right) [62]. In the case of lead in sulphuric acid, the series connection makes more sense because the $PbSO_4$ film is described as a continuous film in literature. Ma et al. [63] modelled the lead-sulphate film that forms in the PbO region[6] with a RC parallel circuit in series. A similar film has also been reported for the positive electrode [45,64], but as the active surface of the positive electrode is larger [45], it does not influence the spectrum significantly. In fact, a small capacitive semicircle at high frequencies can sometimes be observed at the positive electrode.

Fig. 12 shows simulated spectra for a continuous coating (Fig. 11, left), charge transfer with coupled adsorption and series inductance. Simulations with discontinuous coating (Fig. 11 right) have a similar shape. Comparison with Figs. 2 and 3 indicates that the general shape of the negative-electrode impedance spectrum can be reproduced. However, the inductive semicircle is too small in the simulation compared to the measurements. In the measured spectra, the inductive semicircle has about the same diameter as the

[5] Some authors [45,71] have suggested that under certain conditions, charge transfer takes place in two steps, one for each electron. However, the first step is considered to be fast and not creating a semicircle, so only the second one is visible in the spectrum.

[6] There are three potential regions called after the main surface material that forms on lead: the $PbSO_4$ potential region from −0.956 to about −0.3 V vs. Hg/Hg_2SO_4, the PbO region from −0.3 to 0.9 V and the PbO_2 region for potentials larger than 0.9 V. Below −0.956 V, the lead surface is not covered [72,73].

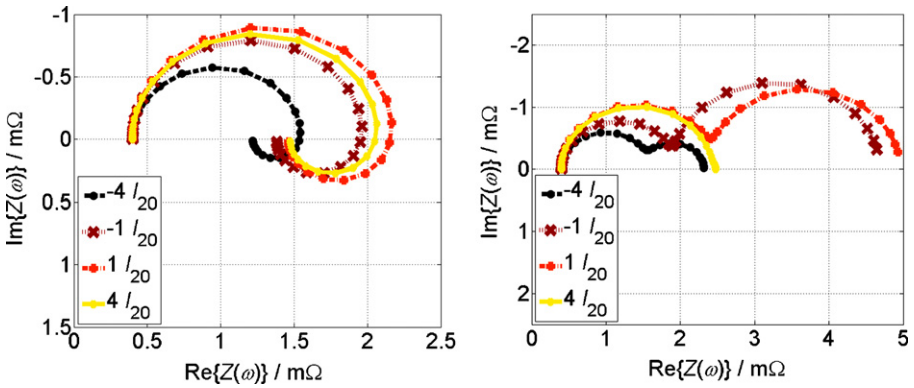

Fig. 9. Simulated spectra of charge transfer with coupled adsorption in parallel to double-layer capacitance, frequency 0.1 mHz to 1 kHz, with $R_0 = 0.4\,m\Omega$, $\alpha = 0.6$, $\beta = 0.5$, $i_0 = 15\,A$, $C_{DL} = 1000\,F$ and variation of k_{ct} and k_{desad}. Left: $k_{ct} = 0.001\,s^{-1}$ and $k_{desad} = 0.005\,s^{-1}$, right: $k_{ct} = 0.005\,s^{-1}$ and $k_{desad} = 0.001\,s^{-1}$.

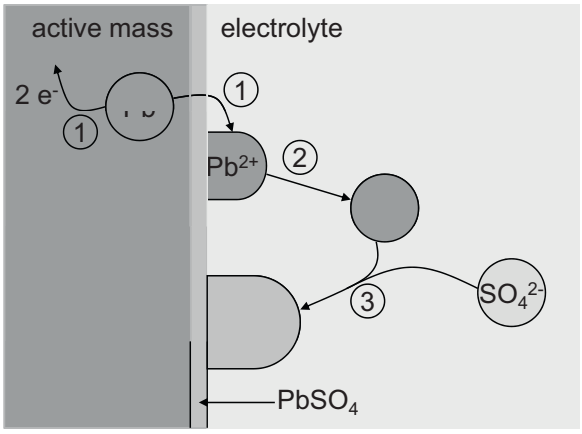

Fig. 10. Course of reaction during discharge as in Fig. 6, but with a thin $PbSO_4$ film.

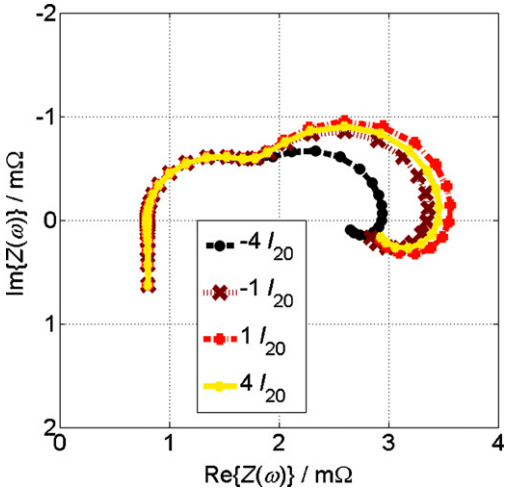

Fig. 12. Simulated spectra of the circuit in Fig. 11 left with an additional series inductance of 10 nH; parameters as in Fig. 9 left and $R_0 = 0.8\,m\Omega$, $R_{coating} = 1\,m\Omega$ and $C_{coating} = 100\,F$.

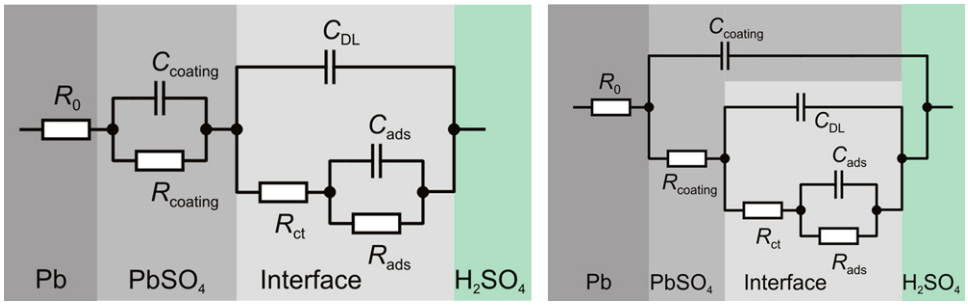

Fig. 11. Equivalent circuits for continuous (left) and discontinuous coatings (right) applied to the negative electrode.

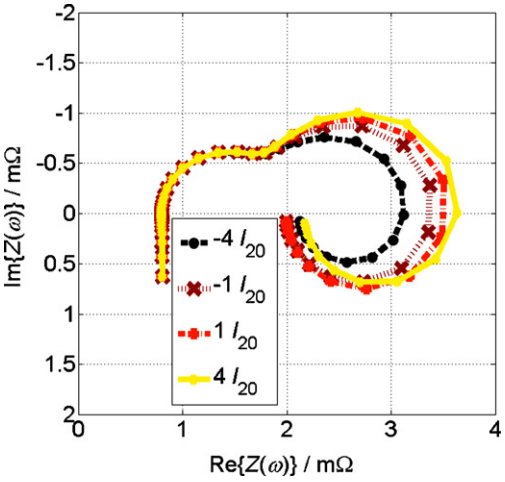

Fig. 13. Simulations with the same parameters as in Fig. 12, but with $n_{ads} = 20$. N_{ct} is not changed ($n_{ct} = 2$).

low-frequency capacitive semicircle, while in the simulation the diameter of the inductive semicircle is only about half the diameter of the low-frequency capacitive semicircle.

The diameter of the inductive semicircle is mainly affected by the adsorption resistance R_{ads} (Eq. (8)) and that of the low-frequency capacitive semicircle by the charge-transfer resistance R_{ct} (Eq. (7)). Looking at the equations, the two resistances are equal if[7]

$$\frac{1}{D(\eta_{DC})} = \frac{A(\eta_{DC})}{D(\eta_{DC}) \cdot (D(\eta_{DC}) \cdot B(\eta_{DC}) - A(\eta_{DC}))} \tag{10}$$

This is fulfilled if $D(\eta_{DC}) \cdot B(\eta_{DC}) = 2A(\eta_{DC})$. $D(\eta_{DC})$ only depends on the charge-transfer parameters i_0, α and n. If only the adsorption resistance is to be changed, then those parameters and consequently $D(\eta_{DC})$ should not be changed. That leaves the parameters k_{desad} and the terms in the exponential function $\beta nF/(RT)\,\eta_{DC}$ and $-(1-\beta)\,nF/(RT)\,\eta_{DC}$. F and R are constants and the temperature T is the same for both charge transfer and adsorption. In the measurements, the diameter of the adsorption semicircle is about the same size as that of the charge-transfer semicircle during both charging and discharging. That also rules out β because changing β would increase the semicircle only for either charging or discharging and decrease it for the other one. The remaining parameters are k_{desad} and the number of elementary charges n_{ads} for adsorption (without changing $n_{ct} = 2$ for charge transfer). $B(\eta_{DC})$ increases with both parameters and the absolute value of $A(\eta_{DC})$ as well ($k_{desad} > k_{ct}$). However, a small increase of k_{desad} is not enough and a large increase removes the adsorption semicircle completely because adsorption is so fast that it does not influence the impedance. Using $n_{ads} \geq 20$ gives the desired result (Fig. 13). The physical interpretation is that charge carriers with a charge of ± 20 electrons are adsorbed. This is of course rather unlikely; so most probably the large diameter of the adsorption semicircle has another origin, e.g. mass transport. Further investigation is necessary, but outside the scope of this paper. It could be helpful to add diffusion of lead ions in the electrolyte and/or lead sulphate layer according to the description of similar processes in [65,66].

[7] For equations of $A(\eta_{DC})$, $B(\eta_{DC})$ and $D(\eta_{DC})$ see Appendix A.

5. Conclusion

This paper proposes an interpretation of the processes causing the different parts of the impedance spectrum of the negative and the positive electrode of lead-acid batteries. The high-frequency capacitive semicircle of the negative electrode has been attributed to the thin lead-sulphate film being formed on the electrode surface and the low-frequency capacitive and inductive semicircle to charge transfer coupled with adsorption of lead ions. The general shape of the measured spectra can be reproduced by simulation, but the diameter of the inductive semicircle does not fit with the measurements, so further investigation on this topic is necessary.

The inductive semicircle occurring at high frequencies in spectra of the positive electrode is probably caused by the reference electrode. Its size changes with SOC, i.e. with changing acid concentration, which fits with findings in literature. To finally prove this theory, more measurements are necessary.

In the second part of this paper, deformation of the spectra due to concentration limitation is investigated.

Acknowledgements

This work was kindly financed by the E.ON International Research Initiative within the project BEST. The authors would like to thank Dr. Eckhard Karden from Ford Research and Advanced Engineering Europe, Aachen, Germany, for valuable discussion.

Appendix A.

$$A(\eta_{DC}) = i_0 \cdot \left(\exp\left(\frac{\alpha nF}{RT}\eta_{DC}\right) + \exp\left(-\frac{(1-\alpha)nF}{RT}\eta_{DC}\right)\right)$$
$$\left[k_{ct}\left(\frac{\alpha nF}{RT} \cdot \exp\left(\frac{\alpha nF}{RT}\eta_{DC}\right) + \underline{\theta}(\omega, \eta_{DC}) \cdot \left(\frac{(1-\alpha)nF}{RT} \cdot \exp\left(-\frac{(1-\alpha)nF}{RT}\eta_{DC}\right) - \frac{\alpha nF}{RT} \cdot \exp\left(\frac{\alpha nF}{RT}\eta_{DC}\right)\right)\right)\right.$$
$$\left. -k_{desad}\left(\underline{\theta}(\omega, \eta_{DC})\left(\frac{\beta nF}{RT} \cdot \exp\left(\frac{\beta nF}{RT}\eta_{DC}\right) - \frac{(1-\beta)nF}{RT}\exp\left(-\frac{(1-\beta)nF}{RT}\eta_{DC}\right)\right) + \frac{(1-\beta)nF}{RT} \cdot \exp\left(-\frac{(1-\beta)nF}{RT}\eta_{DC}\right)\right)\right] \tag{11}$$

$$B(\eta_{DC}) = k_{ct}\left(\exp\left(\frac{\alpha nF}{RT}\eta_{DC}\right) + \exp\left(-\frac{(1-\alpha)nF}{RT}\eta_{DC}\right)\right) + k_{desad}\left(\exp\left(\frac{\beta nF}{RT}\eta_{DC}\right) + \exp\left(-\frac{(1-\beta)nF}{RT}\eta_{DC}\right)\right) \tag{12}$$

$$D(\eta_{DC}) = i_0\left[\frac{\alpha nF}{RT} \cdot \exp\left(\frac{\alpha nF}{RT}\eta_{DC}\right) + \underline{\theta}(\omega, \eta_{DC})\left(\frac{(1-\alpha)nF}{RT} \cdot \exp\left(-\frac{(1-\alpha)nF}{RT}\eta_{DC}\right) - \frac{\alpha nF}{RT} \cdot \exp\left(\frac{\alpha nF}{RT}\eta_{DC}\right)\right)\right] \tag{13}$$

References

[1] E. Karden,Using low-frequency impedance spectroscopy for characterization, monitoring, and modeling of industrial batteries, PhD Thesis, RWTH Aachen University, Institute for Power Electronics and Electrical Drives ISEA, 2001.
[2] F. Huet, Journal of Power Sources 70 (1) (1998) 59–69.
[3] M. Keddam, Z. Stoynov, H. Takenouti, Journal of Applied Electrochemistry 7 (1977) 539–544.
[4] A. Kirchev, F. Mattera, E. Lemaire, K. Dong, Journal of Power Sources 191 (1) (2009) 82–90.

[5] Z. Stoynov, B. Savova-Stoynov, T. Kossev, Journal of Power Sources 30 (1–4) (1990) 275–285.
[6] N. Yahchouchi, Mésure de l'impedance d'un accumulateur tubulaire au plomb: application à la détermination de la capacité électrique, PhD Thesis, Université Pierre et Marie Curie Paris, 1981.
[7] C. Schäper, "Untersuchung des hochfrequenten Impedanzverhaltens von Lithium-Ionen Batterien." Diploma thesis, Institute for Power Electronics and Electrical Drives (ISEA), RWTH Aachen University, unpublished, 2008.
[8] F. Huet, R. Nogueira, P. Lailler, L. Torcheux, Journal of Power Sources 158 (2) (2006) 1012–1018.
[9] F. Huet, R.P. Nogueira, L. Torcheux, P. Lailler, Journal of Power Sources 113 (2) (2003) 414–421.
[10] E. Barsoukov, J.R. Macdonald (Eds.), Impedance Spectroscopy, vol. 2, Wiley-Interscience, 2005.
[11] E. Karden, S. Buller, R.W.D. Doncker, Journal of Power Sources 85 (1) (2000) 72–78.
[12] P. Mauracher, E. Karden, Journal of Power Sources 67 (1–2) (1997) 69–84, Proceedings of the Fifth European Lead Battery Conference.
[13] G. Lindbergh, Electrochimica Acta 42 (8) (1997) 1239–1246.
[14] R. de Levie, Electrochimica Acta 8 (10) (1963) 751–780.
[15] R. de Levie, Electrochimica Acta 9 (9) (1964) 1231–1245.
[16] R. de Levie, Electrochimica Acta 10 (2) (1965) 113–130.
[17] R. de Levie, Advances in Electrochemistry and Electrochemical Engineering 6 (1967) 329–398.
[18] L. Beketaeva, K. Rybalka, Journal of Power Sources 32 (1990) 143–150.
[19] C. D'Alkaine, P. Mengarda, P. Impinnisi, Journal of Power Sources 191 (1) (2009) 28–35.
[20] S.R. Niya, M. Hejabi, F. Gobal, Journal of Power Sources 195 (17) (2010) 5789–5793.
[21] M.P.J. Brennan, B.N. Stirrup, N.A. Hampson, Journal of Applied Electrochemistry 4 (1974) 49–52.
[22] J. Carr, N. Hampson, R. Taylor, Journal of Electroanalytical Chemistry 27 (1970) 201–206.
[23] P. Casson, N.A. Hampson, M.J. Willars, Journal of Electroanalytical Chemistry 97 (1) (1979) 21–32.
[24] N.A. Hampson, S. Kelly, K. Peters, Journal of Applied Electrochemistry 11 (1981) 751–763.
[25] S. Kelly, N.A. Hampson, K. Peters, Journal of Applied Electrochemistry 11 (1981) 765–769.
[26] S. Kelly, N. Hampson, S. Karunathilaka, R. Leek, Surface Technology 13 (1981) 349–355.
[27] M. Keddam, C. Rakotomavo, H. Takenouti, Journal of Applied Electrochemistry 14 (1984) 437–448.
[28] A. Kirchev, A. Delaille, M. Perrin, E. Lemaire, F. Mattera, Journal of Power Sources 170 (2) (2007) 495–512.
[29] S. Chechirlian, P. Eichner, M. Keddam, H. Takenouti, H. Mazille, Electrochimica Acta 35 (7) (1990) 1125–1131.
[30] H. Göhr, M. Mirnik, C.A. Schiller, Journal of Electroanalytical Chemistry 180 (1–2) (1984) 273–285.
[31] G. Hsieh, S.J. Ford, T.O. Mason, L.R. Pederson, Solid State Ionics 91 (3–4) (1996) 191–201.
[32] C.A. Schiller, W. Strunz, Impedanzmessung – Sein oder Schein, in Technische Mitteilungen, vol. 99, pp. 12–18, 1. Symposium Impedanzspektroskopie, Haus der Technik, Essen, May 2006. ISSN 0040-1439.
[33] F. Gutmann, Journal of the Electrochemical Society 112 (1) (1965) 94–98.
[34] R. de Levie, A. Husovsky, Journal of Electroanalytical Chemistry 22 (1) (1969) 29–48.
[35] A. Sadkowski, Journal of Electroanalytical Chemistry 210 (1) (1986) 21–29.
[36] A. Sadkowski, Journal of Electroanalytical Chemistry 447 (1–2) (1998) 97–107.
[37] A. Sadkowski, Journal of Electroanalytical Chemistry 465 (2) (1999) 119–128.
[38] A. Sadkowski, Electrochimica Acta 49 (14) (2004) 2259–2269.
[39] L. Bai, B.E. Conway, Journal of the Electrochemical Society 138 (10) (1991) 2897–2907.
[40] L. Bai, B.E. Conway, Electrochimica Acta 38 (14) (1993) 1803–1815.
[41] M.T.M. Koper, Advances in Chemical Physics XCII (1996) 161–298.
[42] J. Bisquert, H. Randriamahazaka, G. Garcia-Belmonte, Electrochimica Acta 51 (4) (2005) 627–640.
[43] J. Kowal, Spatially-resolved impedance of nonlinear inhomogeneous devices – using the example of lead-acid batteries,PhD Thesis, RWTH Aachen University, Institute for Power Electronics and Electrical Drives ISEA, 2010.
[44] R.D. Armstrong, K.L. Bladen, Journal of Applied Electrochemistry 7 (1977) 345–353.
[45] H. Bode, Lead Acid Batteries, John Wiley & Sons ISBN, 1977, ISBN 0-471-08455-7.
[46] S. Canagaratna, N. Hampson, Journal of Electroanalytical Chemistry 86 (2) (1978) 361–368.
[47] J. Carr, N. Hampson, S. Holley, R. Taylor, Journal of Electroanalytical Chemistry 32 (3) (1971) 345–352.
[48] C. Francia, M. Maja, P. Spinelli, Journal of Power Sources 95 (1–2) (2001) 119–124.
[49] C. Francia, M. Maja, P. Spinelli, Journal of Power Sources 85 (1) (2000) 110–116.
[50] C. Francia, M. Maja, P. Spinelli, F. Saez, B. Martinez, D. Marin, Journal of Power Sources 85 (1) (2000) 102–109.
[51] B.O. Myrvold, Journal of Power Sources 117 (1–2) (2003) 187–202.
[52] D. Pavlov, T. Rogachev, P. Nikolov, G. Petkova, Journal of Power Sources 91 (1) (2009) 58–75.
[53] B. Timmer, M. Sluyters-Rehbach, J. Sluyters, Journal of Electroanalytical Chemistry 18 (1–2) (1968) 93–106.
[54] D. Vanmaekelbergh, B.H. Erne, Journal of the Electrochemical Society 146 (7) (1999) 2488–2494.
[55] D. Pavlov, Electrochimica Acta 13 (10) (1968) 2051–2061.
[56] D. Pavlov, R. Popova, Electrochimica Acta 15 (9) (1970) 1483–1491.
[57] D. Pavlov, Electrochimica Acta 23 (9) (1978) 845–854.
[58] S.B. Hall, G.A. Wright, Corrosion Science 31 (1990) 709–714.
[59] F.E. Varela, M.E. Vela, J.R. Vilche, A.J. Arvia, Electrochimica Acta 38 (11) (1993) 1513–1520.
[60] F.E. Varela, J.R. Vilche, A.J. Arvia, Electrochimica Acta 39 (3) (1994) 401–406.
[61] F.E. Varela, E.N. Codaro, J.R. Vilche, Journal of Applied Electrochemistry 27 (1997) 1232–1244.
[62] M. Schneider, O. Yeserska, and P. Plagemann, "Untersuchung zum Alterungsverhalten von hochohmigen Korrosionsschutzschichten mittels EIS," in Technische Mitteilungen, vol. 99, pp. 46–52, 1. Symposium Impedanzspektroskopie, Haus der Technik, Essen, May 2006, ISSN 0040-1439.
[63] M. Ma, C.-X. Yang, W.-B. Cai, W.-F. Zhou, H.-T. Liu, Journal of The Electrochemical Society 150 (7) (2003) B325–B328.
[64] M. Maja, N. Penazzi, Electrochimica Acta 30 (6) (1985) 773–778.
[65] C. Gabrielli, M. Keddam, F. Minouflet-Laurent, K. Ogle, H. Perrot, Electrochimica Acta 48 (11) (2003) 1483–1490.
[66] A. Sadkowski, Journal of Electroanalytical Chemistry 454 (1–2) (1998) 39–52.
[67] B. A. Boukamp, Impedance spectroscopy, strength and limitations (Impedanzspektroskopie, Stärken und Grenzen), Technisches Messen, vol. 71, September, 2004, pp. 509–518.
[68] M. Urquidi-Macdonald, S. Real, D.D. Macdonald, Electrochimica Acta 35 (10) (1990) 1559–1566.
[69] M. Urquidi-Macdonald, S. Real, D.D. Macdonald, Journal of the Electrochemical Society 133 (10) (1986) 2018–2024.
[70] J. Kowal, D. Hente, D.U. Sauer, IEEE Transactions on Instrumentation and Measurement 58 (2009) 2343–2350.
[71] N. Hampson, J. Lakeman, Journal of Power Sources 4 (1979) 21–32.
[72] D. Pavlov, C.N. Poulieff, E. Klaja, N. Iordanov, Journal of the Electrochemical Society 116 (3) (1969) 316–319.
[73] D. Pavlov, N. Iordanov, Journal of the Electrochemical Society 117 (9) (1970) 1103–1109.